Monolithically integrated widely tunable 40 Gbits/s wavelength converter with optical label modulation function

Wenbin Zhao,[1,*] Milan L. Mašanović,[1] Daniel J. Blumenthal,[1] and Gregory Fish[2]

[1]*Department of Electrical and Computer Engineering, Optical Communication and Photonic Networks Group, University of California, Santa Barbara, California 93106, USA*

[2]*JDSU, 475 Pine Avenue, Santa Barbara, California 93117, USA*

[*]*Corresponding author: wzhao@luminentoic.com*

Received February 23, 2007; revised June 6, 2007; accepted June 19, 2007; published July 24, 2007 (Doc. ID 80389)

What we believe to be a novel monolithically integrated wavelength converter consisting of a sampled grating distributed Bragg reflector laser, a long semiconductor optical amplifier (SOA), and a delayed interferometer Mach–Zehnder interferometer (DIMZI) is reported. Error-free 40 Gbits/s wavelength conversion for three different probe wavelengths is demonstrated. The impact of the output filter bandwidth and filter detuning on the performance of wavelength conversion is studied in detail. The optical label modulation of the on-chip DI-MZI is first demonstrated with amplitude- and phase-shift key schemes. © 2007 Optical Society of America

OCIS codes: 130.3120, 250.5980.

1. Introduction

An optical packet switching network with a bandwidth of more than hundreds of terabits per second is a promising network architecture to meet future demands [1,2]. Tunable all-optical wavelength conversion (AOWC) and optical label processing are key functions in this optical packet switching network. Optical information processing (IP) data packets are generally routed through this all-optical network to the destination by switching the packet carrier's wavelengths. Optical labels carry all forwarding information for traffic engineering. Integration of the packet forwarding functions, such as optical label erase, wavelength conversion, and optical label write on a single chip, is expected to improve the performance of optical packet switching while making it more cost effective [3,4]. The wavelength converter design is critical to the performance of the packet switching and its cascadability. The optical label modulation is also very important for label swapping and packet forwarding.

In this paper, we report on the design and 40 Gbits/s error-free performance of what we believe is a novel monolithic tunable optical wavelength converter consisting of a sampled grating distributed Bragg reflector (SGDBR) laser and a delayed-interference wavelength converter (DIWC). We study the impact of external output filtering on the wavelength converter's performance. In that respect, we characterize the effects of the optical filter's bandwidth on the converted eye opening and extinction ratio, and the effect of filter detuning between the filter peak position and the probe cw peak. In addition, we characterize the delayed-interference Mach–Zehnder interferometer (DI-MZI) as either intensity or phase modulator for 10 Gbits/s serial optical label coding. The optical packet is assumed with 40 Gbits/s payloads and 10 Gbits/s serial labels [1]. The integrated DIWC chip has the entire packet forwarding functions. This study is of general interest and it is applicable to any DIWC-based device.

2. Device Design and Test Setup

The schematic of the tunable wavelength converter is shown in Fig. 1(a). The cw probe signal is generated by an on-board SGDBR laser, amplified by the booster semiconductor optical amplifier (SOA) and fed to the DIWC SOA through a 2×1 multiple

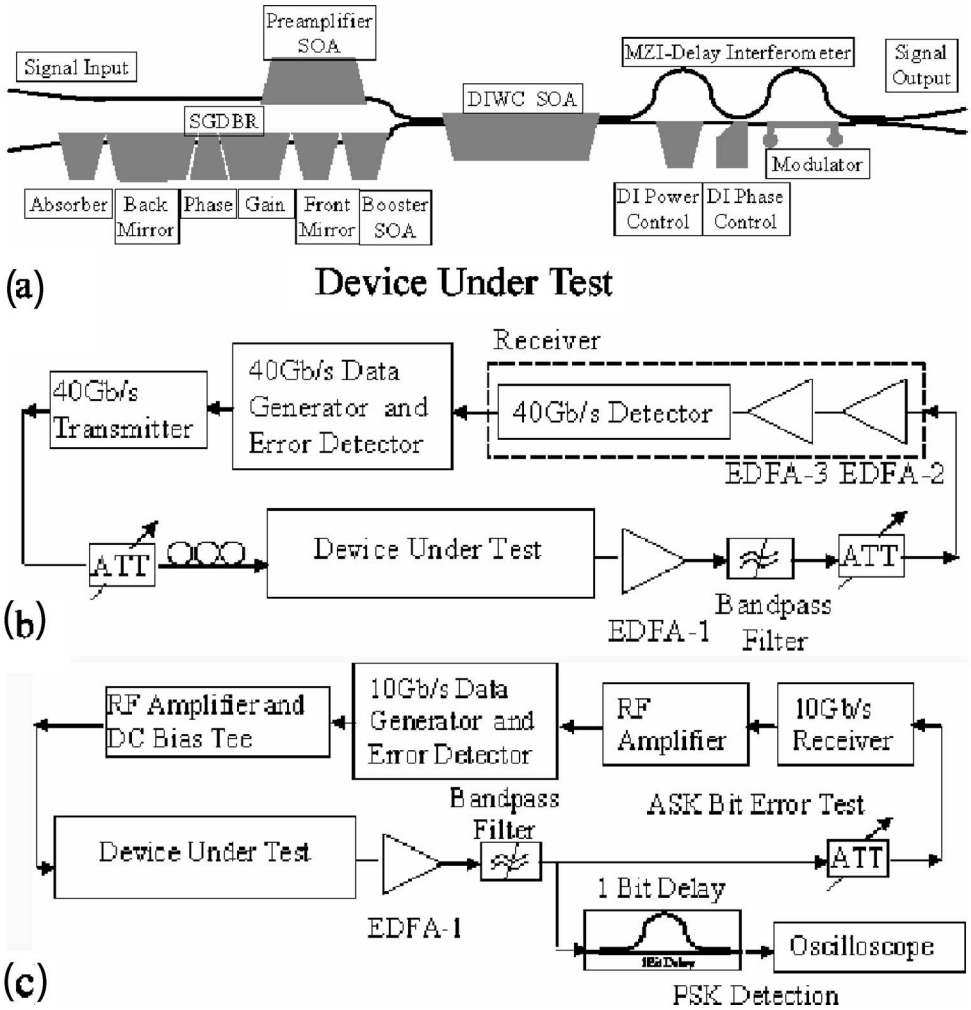

Fig. 1. (a) Schematic of the integrated wavelength converter. (b) Test setup used for the characterization of wavelength conversion. (c) Test setup used for the characterization of DI-MZI optical label modulation.

mode interference (MMI) coupler. The pump signal is coupled onto the chip through an angled and tapered input waveguide, amplified by a preamplifier, and then coupled to the DIWC SOA by the 2×1 MMI coupler. The DIWC SOA is 1.5 mm long, followed by a 2×2 MMI coupler whose outputs form the front end of a passive MZI. One arm of the MZI is longer than the other, introducing a differential 10 ps signal delay. The optical power in the shorter arm and the phase difference between the two arms can be independently controlled by biasing phase and power electrodes on the passive waveguide. A third electrode shown in Fig. 1(a) is used for the electrical signal modulation for optical label coding. The device is fabricated using the offset quantum well integration platform described in [5], with the addition of a deeply etched delay waveguide. The whole chip size is approximately 0.8×7 mm^2.

Figure 1(b) shows the test setup of the wavelength conversion. Return-to-zero (RZ) data is generated by externally modulating 3.5 ps output pulses from a mode-locked ring laser with a 40 Gbits/s modulator, which is driven by a superhyperfine (shf) 40 Gbits/s bit error rate test (BERT) with 2^7-1 pseudorandom bit sequence (PRBS) data. The RZ signal wavelength is at 1552.2 nm. The input data's pulse width is measured by an autocorrelator. The data are coupled on and off the chip using lensed fibers. The input data introduce cross-phase modulation (XPM) onto the probe signal, and the DI-MZI performs the function of a gate driven by the chirp introduced into the probe signal by the pump signal [4,6,7]. At the output of the device, the signal wavelength is selected by a narrow-pass-band filter, which also plays a role in pulse reshaping. The receiver consists of a cascade of two erbium-doped fiber amplifiers (EDFAs), followed by a 40 GHz photodiode. A back-to-back bit error rate (BER) curve is measured before the receiver.

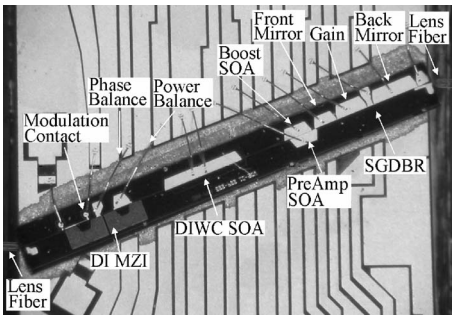

Fig. 2. Photo of the device under test.

Figure 1(c) shows the test setup of the DI-MZI modulator for the serial optical label. The on-chip SGDBR, booster SOA, and DIWC SOA are all set to the same operation conditions as their wavelength conversion functions. A signal with $2^{31}-1$ PRBS data is boosted by an amplifier and biased by a bias tee, then coupled to the chip by a coplanar probe. The modulation signal's amplitude on the chip is estimated at ~ -1.8 V for the intensity modulation and -3.1 V for the phase modulation. The modulator's electrode is the push-pulled design with a 50 Ω termination resistor and a capacitor. At the chip's output, the EDFA and band-pass filter have the same setup as its wavelength conversion function. In an amplitude shift key (ASK) modulation scheme, the output signal is sent directly to the receiver for bit error measurement. For a phase shift key (PSK) modulation scheme, a 1 bit delay DI-MZI is built by two couplers with a 2.1 cm length differential between two arms, converting the phase signal to the intensity signal. Figure 2 shows the device under test.

3. Principle and Performance of Wavelength Conversion

The principle of the DIWC has been explained in detail in [4,8]. Figure 3 shows the transition of the modulated dark pulse to the RZ pulse through the DI-MZI. The cw light is modulated by cross-gain modulation (XGM) and XPM when both the cw and the signal propagate through a long SOA. The DI-MZI plays a role as a gate to convert a chirped dark pulse to an RZ pulse at the destruction output port. Due to the nature of the DIWC, an imperfect cancellation of the power leads to a poor output extinction ratio (ER), which is determined by the input pulse width and the differential time between the two arms of the DI-MZI. In Fig. 3, the RZ intensity pulse at the destruction port has a small power residual hump, which penetrates into the next bit slot and degrades the extinction ratio of the eye diagram. To counteract this inherent drawback of the DIWC, an external bandpass filter is used at the output to achieve a higher extinction ratio.

The XGM after a single Gaussian pulse passing through the SOA can be modeled as

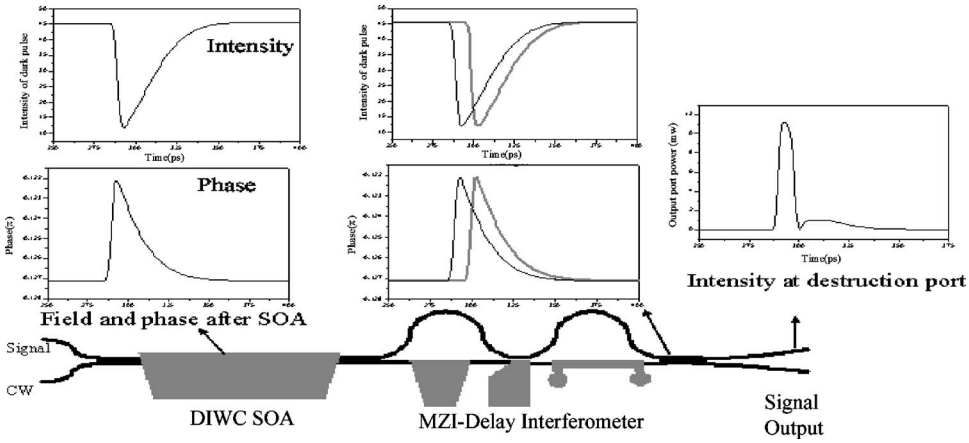

Fig. 3. Operation principle of the DI-MZI based wavelength conversion.

$$G(\tau)=\begin{cases} G_0\exp(-(G_{CW}-1)P_{CW}/P_{SAT}) & \tau\le -1.665\tau_0 \\ \dfrac{1}{\{1-(1-1/G_0)\exp[-U_{SIG}(\tau)/E_{SAT}]\}} & -1.665\tau_0\le\tau\le 1.665\tau_0, \\ \bar{G}_0\exp[-\ln(\bar{G}_0/G_f)\exp(-\tau/\bar{\tau}_C)] & \tau\ge 1.665\tau_0 \end{cases} \quad (1)$$

where G_0 is the small signal gain over the SOA's length,

$$G0=\exp\left(\int g_0 dz\right), \quad (2)$$

G_{cw} is the cw gain, P_{cw} is cw input power to the DIWC SOA from the SGDBR, and P_{SAT} is the cw saturation power. $E_{sat}=\hbar\omega 0wd/\Gamma a$ is the signal saturation energy. Γ is the overlap integral confinement factor between the field mode and the carrier recombination area. a is the differential modal gain, and wd is the cross-section area. $\bar{G}_0=G_0/(1+P_{cw}/P_{SAT})$ is the effective small signal gain. $\bar{\tau}_C=\tau_C/(1+P_{cw}/P_{SAT})$ is the effective carrier lifetime, which is the factor limiting the high-speed operation of the SOA. The estimated carrier lifetime of this device is more than 60 ps. $U_{sig}(\tau)$ is the input signal's integral energy,

$$U_{sig}(\tau)=\int_{-\infty}^{\tau} P_{SIG}(\tau)d\tau, \quad (3)$$

$$P_{sig}(\tau)=\frac{E_{SIG}}{\tau_0\sqrt{\pi}}\exp\left(-\frac{\tau^2}{\tau_0^2}\right), \quad (4)$$

is the input Gaussian signal, and τ_0 is the pulse width. The XPM and XGM are always coherent together by Kramers–Krönig relation, which can be simply modeled by

$$\frac{\partial\phi}{\partial z}=-\frac{1}{2}\alpha_N g, \quad (5)$$

where α_N is the linewidth enhancement factor. Figure 4 is the XGM dark pulse from Eq. (1).

The dark pulse's fall time is determined by the input signal's pulse width, and its recovering time is determined by the material gain recovery and the carrier injection. The transfer function of the DI-MZI can be written as

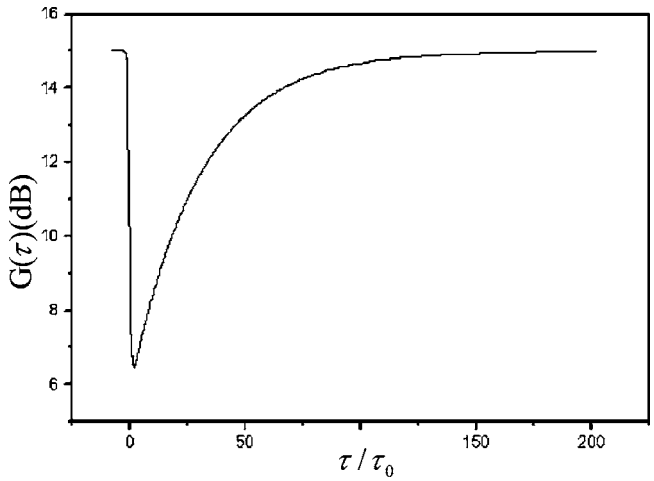

Fig. 4. XGM dark pulse shape calculated from the close form (1).

$$T_{DI\text{-}MZI}(t) = \begin{bmatrix} -\frac{i}{2}P_{in}(t-\Delta t)\exp(ik\Delta L) + \frac{1}{2}P_{in}(t)\exp[-\alpha(I,V) + i\Delta\phi(I,V)] \\ \frac{1}{2}P_{in}(t-\Delta t)\exp(ik\Delta L) - \frac{i}{2}P_{in}(t)\exp[-\alpha(I,V) + i\Delta\phi(I,V)] \end{bmatrix}, \quad (6)$$

where P_{in} is the input power of the DI-MZI, ΔL is the length difference between the two arms, and $\Delta t = \Delta L/c$. The absorption coefficient α and the phase change $\Delta\phi$ are adjusted and modulated by both the injection current on one of the contact pads and the reverse bias and on the others. At the two output ports of the DI-MZI the converted output signal $P_{CONVERTED}$ of the destruction port and the bit inverted signal $P_{INVERTED}$ of the construction port are

$$P_{CONVERTED} = |T_{DI\text{-}MZI}|_1^2 G(\tau) P_{CW},$$

$$P_{INVERTED} = |T_{DI\text{-}MZI}|_2^2 G(\tau) P_{CW}, \quad (7)$$

where P_{CW} is the output power of the SGDBR on the chip. The converted RZ's pulse width and extinction ratio at the destruction port of the DI-MZI are related to the input signal's pulse width and the time differential between two arms of DI-MZI in Fig. 3.

Optimized operating conditions of the device are obtained with the SGDBR gain biased at 110 mA, cw booster SOA at 45 mA, preamplifier SOA at 100 mA, and DIWC-SOA at 475 mA. The signal input power is 5 dBm in fiber, with a coupling loss of approximately 6 dB. The probe signal power generated by the SGDBR is estimated at ~9.5 dBm, which generates ~5.5 mA photocurrent in the reverse-biased DIWC-SOA. The tuning range of SGDBR is ~33 nm from 1534.51 nm to 1567.42 nm (Fig. 5).

Electric current is injected into the phase balance contact on one arm of the DI-MZI to change the material's index and thus reverse the signal's phase at the output coupler. The phase current is varied with the different probe wavelengths. The DI-MZI power balance electrode is used to balance the power at the output coupler from the two arms of the DI-MZI by electroabsorption under reverse bias. Figure 6 shows the output power with the phase current injected on the phase balance electrode at various reverse biases on the power balance electrode. At zero volt bias, the phase current should be 2.25 mA to make one of the output ports fully destructed.

The extinction ratio and pulse width of the converted RZ signal are also related to the gain recovery and time differential of the DI-MZI. The short input pulse width (3.5 ps) short delay (6 ps) would make a better extinction ratio. For our device with a 10 ps differential delay between the two arms of the DI-MZI, the recovery trails of the dark pulses from the two arms cannot cancel well at the MMI of the DI-MZI. The residual power greatly damages the extinction ratio. The converted signal extinction ratio is poor without the assistance of the narrow filter because of the way the DIWC

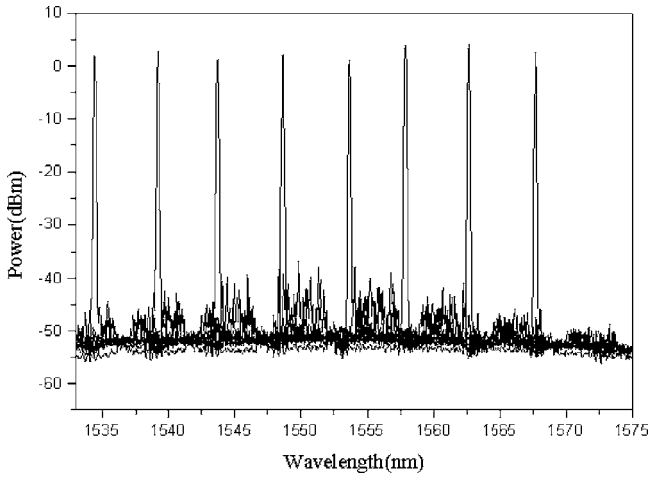

Fig. 5. Measured tuning spectra of the integrated SGDBR.

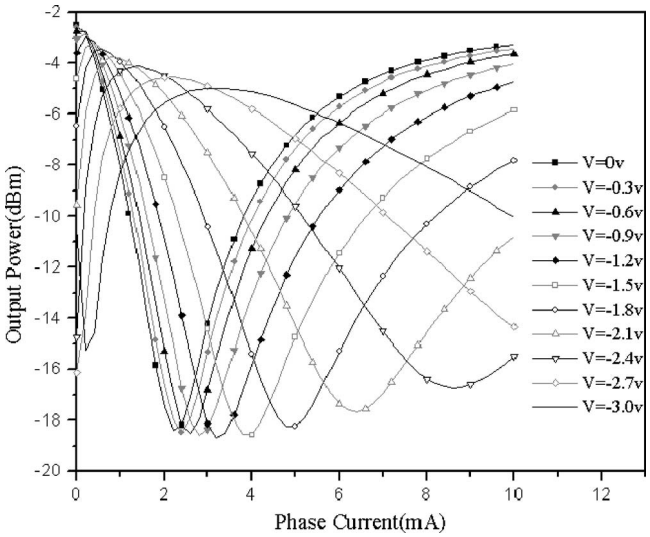

Fig. 6. Measured output power at the destruction port of the DI-MZI versus the phase current on the phase balance contact at the different bias on the power balance contact.

operates. Besides providing pump signal filtering at the device output, the narrow filter at the output also reshapes the converted pulse and greatly improves the extinction ratio.

Figures 7(a)–7(c) show the eye diagrams obtained with filter bandwidths of 1.2, 0.6, and 0.4 nm, respectively. With the 1.2 nm external filter, the converted signal power level is high (approximately −10 dBm after coupling). However the zero power level is also very high, which makes the extinction ratio very poor. The eye in Fig. 7(b) has an extinction ratio measured to be 10 dB while the extinction ratio in Fig. 7(c) was measured to be 11.5 dB. The narrow bandwidth of the 0.4 nm filter does improve the eye opening and reduce the pattern dependence. However, intersymbol interference (ISI) at one level is visible due to the pattern dependence in Fig. 7(c). Evaluating the bit error of the wavelength conversion through the device, the best performance was obtained for the 0.4 nm filter at the output, and all the bit error measurement results presented in this paper were obtained with this particular filter bandwidth.

Figure 8(a) shows the overlapped spectra of the probe signal with no data modulation, a probe signal with the data going through the device, and the converted data signal with the optimum position of the external filter. In order to optimize the performance of the device, we investigated the converted signal extinction ratio as a function of the external filter detuning. We define the difference between the filter peak position and the cw probe wavelength as frequency detuning. The results of this study are shown in Fig. 8(b). The highest extinction ratio is obtained for the filter detuning of 0.25 nm toward the lower wavelength. Moving spectrally to the right from this optimum operation point, the zero level of the pulses increases, thus reducing the extinction ratio. This is indicated by the sharp fall of the extinction ratio in Fig. 8(b). Moving spectrally to the left of the peak in Fig. 8(b), the output power is reduced, thus reducing the one level of the pulses, inducing a moderate rolloff of the extinction.

The XPM generates the large chirp on the converted pulse due to the carrier density and gain modulation in the DIWC-SOA. Since the ratio of the input pulse width and gain recovery time is very small ($\tau_0/\tau_C \approx 0.025$), the nonlinearity induced by the modulation is very strong [9,10]. In the frequency domain, the chirped signal induces the blueshifted sideband next to the probe carrier wavelength. From the spectra in Fig. 8(a), a great deal of energy is pushed into the sideband due to the chirp. The probe wavelength carries the dark pulse signal, and its sideband carries the RZ pulse data. The narrow filter, with the detuning of the filter's peak from the probe wave-

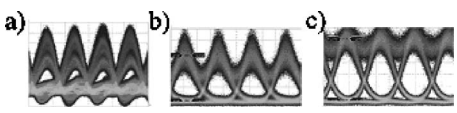

Fig. 7. Eye diagrams with different external filter bandwidths a) 1.2, b) 0.6, and c) 0.4 nm. The wavelength is 1536.43 nm.

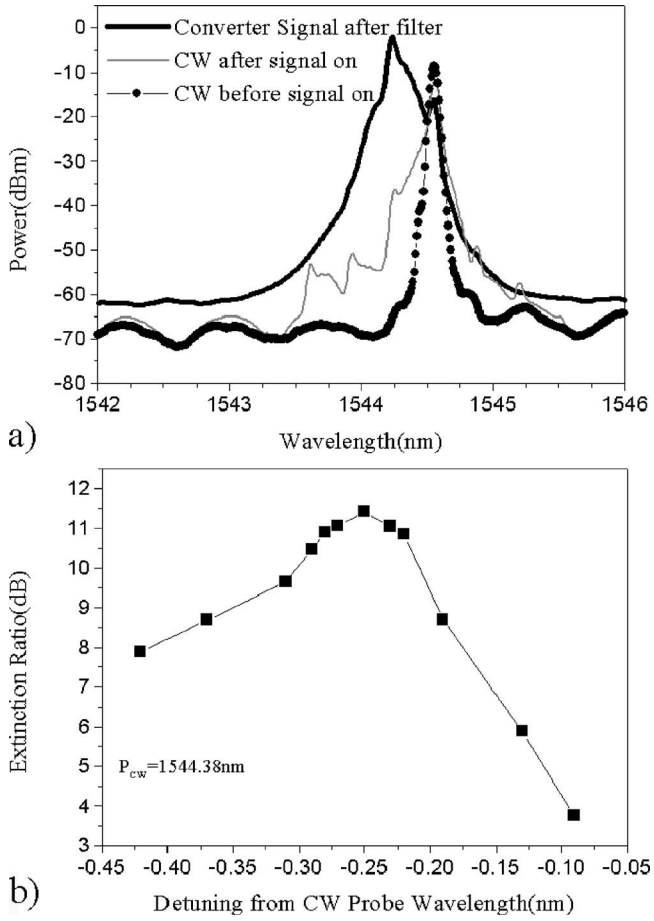

Fig. 8. a) Overlapped spectra at the wavelength converter's output. (b) Measured extinction ratio as the function of filter detuning.

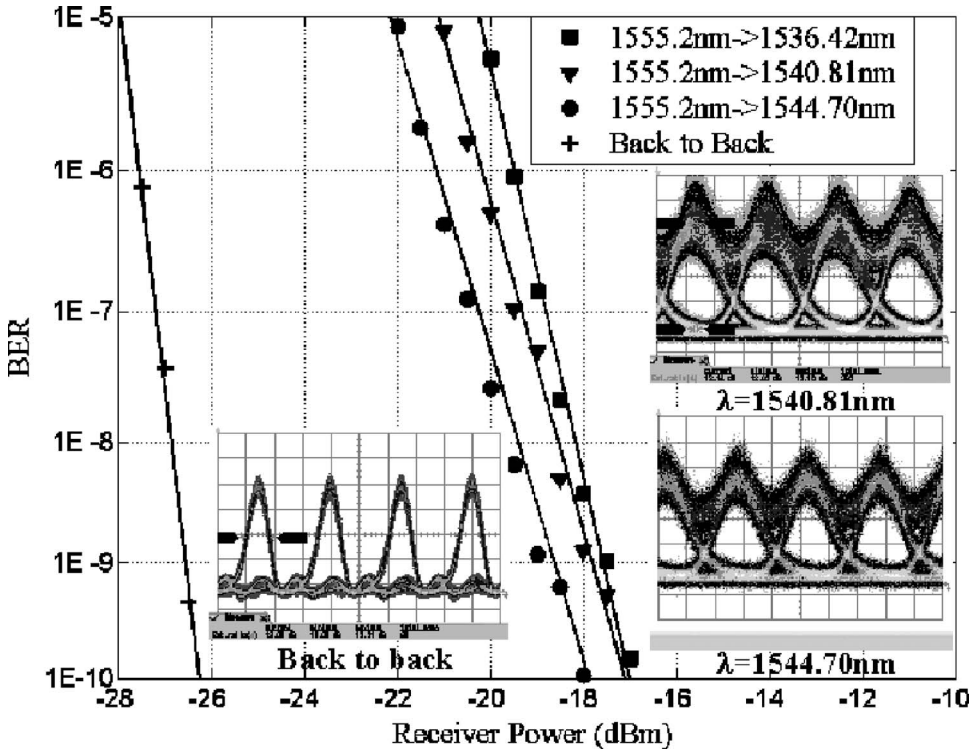

Fig. 9. Bit error measurement results for three different output wavelengths with a 0.4 nm filter at the output.

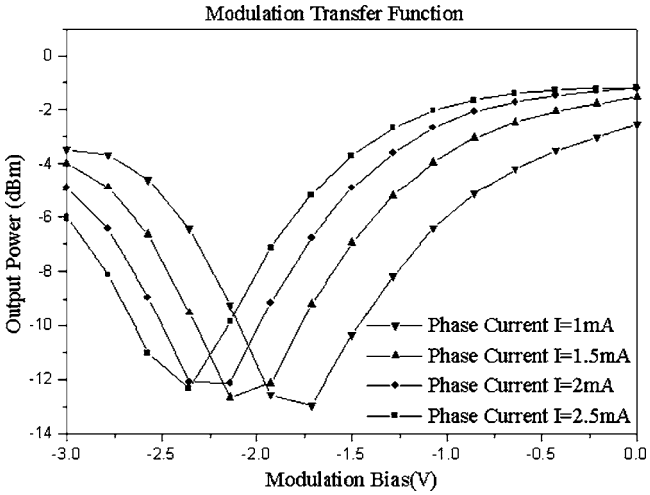

Fig. 10. Measured transfer functions of the DI-MZI modulator.

length (cw) can suppress the dark pulse signal, and takes off the RZ signal, thus reshaping the pulse and improving the extinction ratio.

Figure 9 shows the BER curves for three different output wavelengths. A back-to-back BER curve was measured at 1552.2 nm. The power penalties are between 7.7 dB and 8.8 dB at BER$=10^{-9}$. The main reason for this high penalty is the poor residual power cancellation of the DI-MZI, and low conversion efficiency of the DIWC-SOA. The preamplifier SOA induces many pattern effects that contribute to the large power penalty. The large coupling loss of the MZI structure results in the low optical signal to noise ratio at the output of the chip. The peak power of the wavelength converted signal is approximately −10 dBm before external filtering. After filtering, the power level drops to ∼−20 dBm. Finally, intersymbol interference (ISI) induced by pattern dependence also greatly increases the penalty.

4. Optical Label Modulation

Optical label modulation is the other function of this monolithically integrated optical DIWC chip. The DI-MZI is characterized as a modulator with a 10 Gbits/s optical label rewrite function for packet forwarding.

Figure 10 shows the measured modulation transfer function of the DI-MZI. The reverse bias is added on the modulator's push-pulled designed electrode, and the

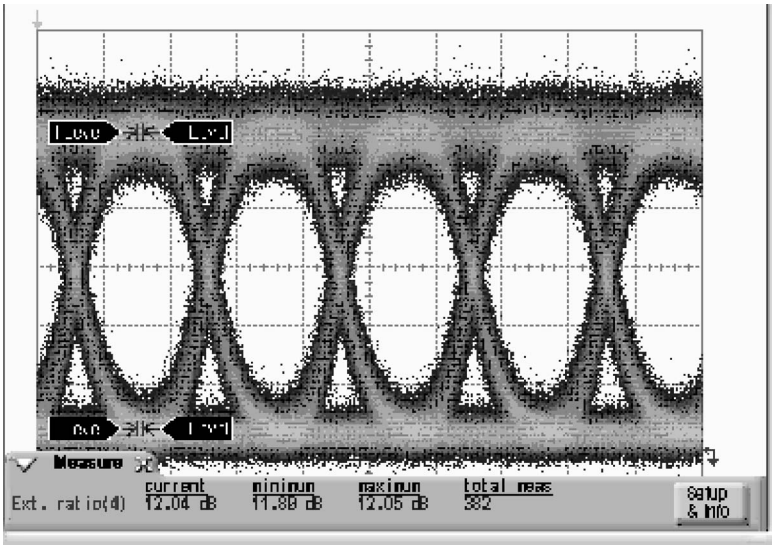

Fig. 11. 10 Gbits/s intensity modulated eye diagram.

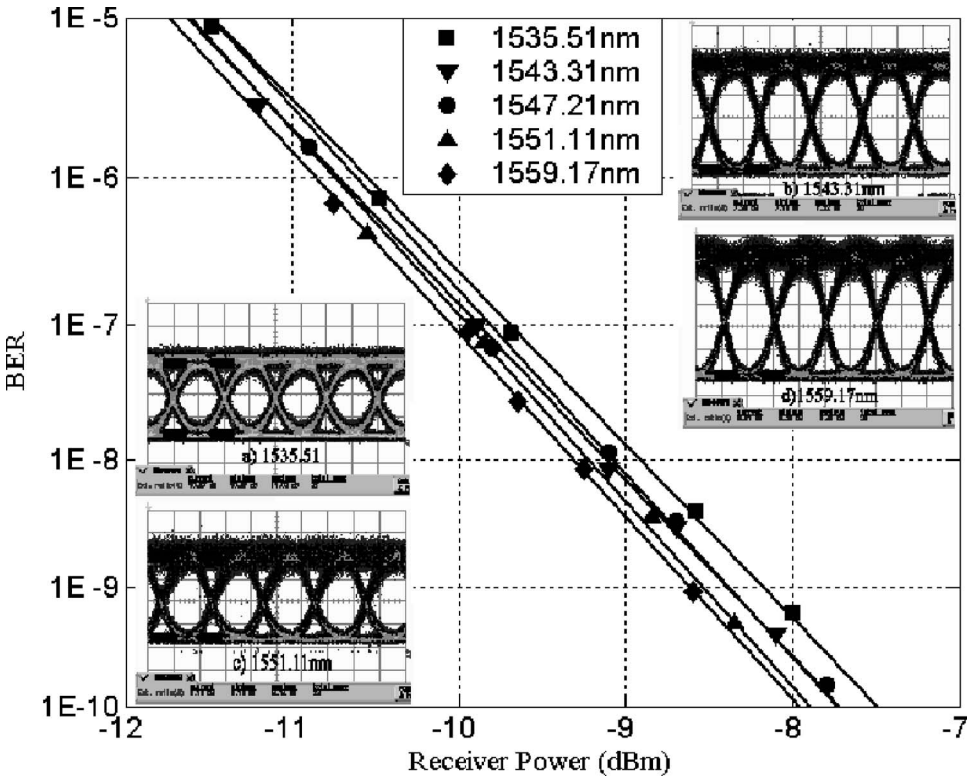

Fig. 12. Bit error measurement of five tuning wavelengths of SGDBR.

phase current is injected on the phase balance electrode to add extra phase to fine-tune the transfer function. The extinction ratio is more than 12 dB with a 1.8 V reverse bias and 1 mA phase current.

Figure 11 shows the 10 Gbits/s eye diagram modulated at a 1547.21 nm wavelength. The extinction ratio is 12.04 dB. The passive waveguide of the DI-MZI is 1.4 Q material. Under the reverse-biased modulation, the material's electroabsorption is very high, and the index is also changed inducing the phase differential between the two arms. From the transfer functions in Fig. 10, when the bias is −3 V, the field's phase change is close to π, and the intensity at the destruction port is ~3 dB less compared with the intensity at zero bias. Therefore, the phase-induced intensity modulation dominates over the electroabsorption modulation. Both effects make the extinction ratio very high. The bit error of five wavelengths covering SGDBR's tuning range is measured in Fig. 12.

The other modulation scheme, differential PSK (DPSK), is very attractive for the serial optical label coding in optical packet switching network architecture [11,12]. Since XGM/XPM is intensity (photon number) driven modulation, the signal's phase doesn't play any role during wavelength conversion. Therefore, when the packet of 10 Gbits/s DPSK serial label and 40 Gbits/s payload passes through the wavelength converter, the optical label can be erased automatically. The DI-MZI functions as a phase modulator [13] to rewrite the label onto the payload after a wavelength conversion. Figure 13 shows the transition from intensity modulation to phase modulation by injecting current to fine-tune the transfer function. The intensity modulated eye diagram in Fig. 13(a) is changed to the intensity signal eye with a π phase shift field in Fig. 13(b) by increasing the phase current. Figure 13(b-1) is the PSK intensity signal eye diagram detected from one port of a 1-bit delayed MZI. Increasing phase current more, the PSK signal eye is switched back to intensity signal eye. Therefore, the DI-MZI can code the DPSK phase modulation scheme for the serial optical label.

5. Conclusion

We have demonstrated a novel widely tunable monolithically integrated wavelength converter, with error-free operation at 40 Gbits/s RZ. We also studied the impact of the external output filtering on the wavelength converter's performance. The best per-

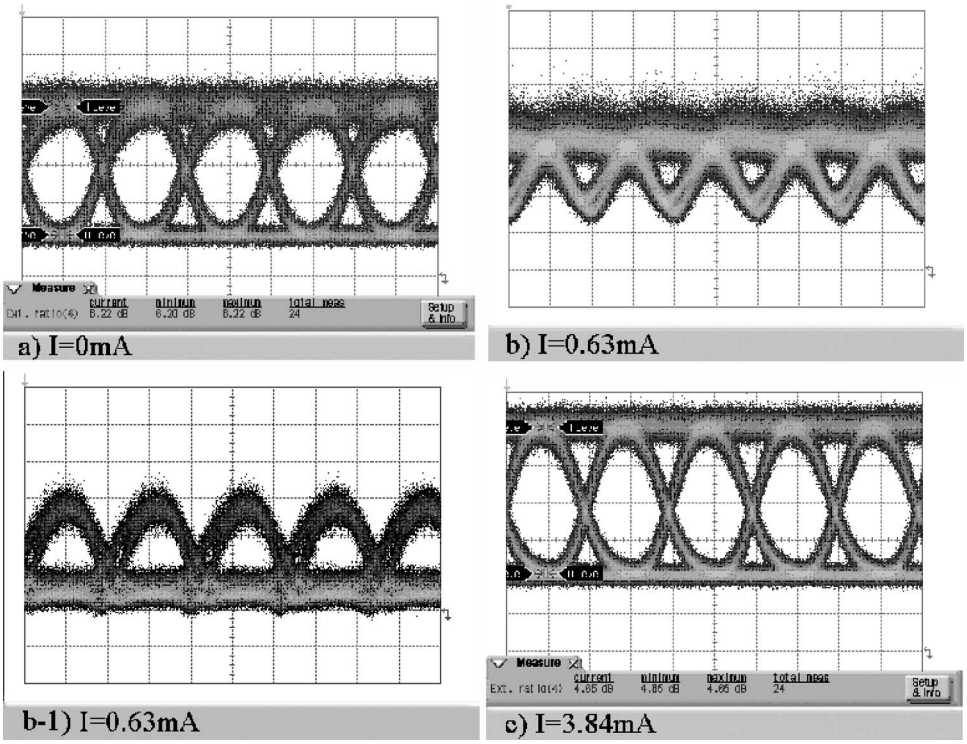

Fig. 13. Transition from intensity modulation to PSK modulation.

formance was obtained by using a 0.4 nm wide filter. To obtain the highest extinction ratio, it was necessary to detune the filter to a shorter wavelength by 0.25 nm. The high power penalty observed is due to the low conversion efficiency, pattern effects, and imperfect residual power cancellation of the DI-MZI. Increasing the SOA's length for the stronger XGM/XPM [9], and optimizing the design of DI-MZI to align the tail power level of two dark pulses for better power cancellation can reduce the penalty. In addition, the 10 Gbits/s modulation of the ASK and PSK scheme for an optical label rewrite is also demonstrated. The DPSK modulation scheme of the DI-MZI still needs more optimization and a subsystem test. Therefore, the integrated chip will have full capacity to handle the optical label in an all-optical core router.

References

1. D. J. Blumenthal and M. Masanovic, "LASOR (label switched optical router): architecture and underlying integration," in *ECOC 2005* (IEEE, 2005), Vol. 5, pp. 25–29.
2. D. Wolfson, V. Lal, M. Mašanović, H. N. Poulsen, and D. J. Blumenthal, "All-optical asynchronous variable-length optically labelled 40 Gbits/s packet switch," in *ECOC 2005* (IEEE, 2005), Vol. 6, pp. 49–50.
3. V. Lal, M. L. Mašanović, D. Wolfson, and D. J. Blumenthal, "Monolithic widely tunable optical packet forwarding chip in InP for all-optical label switching with 40 Gbits/s payloads and 10 Gbits/s labels," *ECOC 2005* (IEEE, 2005), Vol. 6, pp. 25–26.
4. P. Bernasconi, W. Yang, L. Zhang, N. Sauer, L. Buhl, I. Kang, S. Chandrasekhar, and D. Neilson, "Monolithically integrated 40 Gbits/s wavelength converter with multi-frequency laser," in *OFC 2005* (Optical Society of America, 2005), PDP16.
5. M. L. Mašanović, V. Lal, J. S. Barton, E. J. Skogen, J. A. Summers, L. Rau, L. A. Coldren, and D. J. Blumenthal, "Widely-tunable monolithically-integrated all-optical wavelength converters in InP," J. Lightwave Technol. **23**, 1350–1362 (2005).
6. J. Leuthold, J. Jaques, and S. Cabot, "All-optical wavelength conversion and regeneration," in Optical Fiber Communication Conference, OFC 2004 (Optical Society of America, 2004), Vol. 1, pp. 23–27.
7. J. Leuthold, D. M. Marom, S. Cabot, J. J. Jaques, R. Ryf, and C. R. Giles, "All-optical wavelength conversion using a pulse reformatting optical filter," J. Lightwave Technol. **22**, 186–192 (2004).
8. W. Xing, J. Leuthold, and L. Zhang, "Delay-interferometer-based optical pulse generator," in *Optical Fiber Communication Conference, OFC 2004*, (Optical Society of America, 2004), Vol. 1, pp. 23–27.
9. W. Zhao, Z. Hu, V. Lal, L. Rau, and D. J. Blumenthal, "Optimization of ultra-long MQW semiconductor optical amplifiers for all-optical 40-Gb/s wavelength conversion," in *Devices*

for Optical Communication, CLEO (IEEE, 2005), pp. 1426–1428.
10. G. P. Agrawal and N. Anders Olsson, "Self-phase modulation and spectrum broadening of optical pulses in semiconductor laser amplifiers," IEEE J. Quantum Electron. **25**, 2297–2306 (1989).
11. N. Chi, L. Xu, J. Zhang, P. V. Holm-Nielsen, C. Peucheret, Y. Geng, and P. Jeppesen, "Transmission and optical label swapping for 40 Gbits/s WDM signals deploying orthogonal ASK/DPSK labeling," IEEE Photon. Technol. Lett. **17**, 1325–1327 (2005).
12. X. Liu, X. Wei, Y. Su, J. Leuthold, Y.-H. Kao, I. Kang, and R. C. Giles, "Transmission of an ASK-labeled RZ-DPSK signal and label erasure using a saturated SOA," IEEE Photon. Technol. Lett. **16**, 1594–1597 (2004).
13. A. H. Gnauck and P. J. Winzer, "Optical phase-shift-keyed transmission," J. Lightwave Technol. **23**, 115–124 (2005).